

Effect of composite pore-forming agent on the performance of fly ash ceramic membrane support

Wenhao Shi, Yani Guo*, Weixing Chen, Xiaoyu Yang, Yuhong Zhou and Zhigang Wang

School of Environmental and Chemical Engineering, Xi'an Polytechnic University, Xi'an 710600, China

In order to prevent the problem of fracture of ceramic membrane supports during sintering due to excessive sintering losses, the effects of sintering temperature, composite pore-forming agent content and heating rate on the supports were thoroughly investigated. The results show that compared with a single pore-forming agent, the composite pore-forming agent can prevent its own rapid decomposition and widen the temperature range, thus it is easier to prepare the ceramic membrane support with high permeability. When the sintering temperature was 1020.69 °C, the composite pore-forming agent content was 11.46 wt%, and the heating rate was 10 °C/min, the optimal support was prepared with a pure water flux of 2983.81 L/(m²·h·MPa), a flexural strength of 31.27 MPa, and an average pore size of about 1.88 μm. This method can greatly shorten the firing cycle without compromising the support qualities, since these properties are mainly affected by the amount of pore-forming agent rather than the heating rate. According to acid and alkali corrosion experiments, the fly ash-based support body has good resistance to acid and alkali corrosion. Therefore, the addition of a composite pore-forming agent is a feasible method to produce high-flux, high-porosity ceramic membrane supports and rapid firing, and the obtained supports are compatible with the application conditions of porous ceramic materials.

Keywords: Fly ash, Ceramic membrane supports, Composite pore-forming agent, Quick firing, Response surface methodology.

Introduction

Porous inorganic ceramic membranes are widely used in various industries, including petrochemicals [1], environmental protection [2], food [3], and medicine [4], due to their superior material stability. They are also one of the fastest advancing membrane materials with the most potential [5]. Before utilization [6], a support with sufficient flexural strength is required due to low elasticity and brittleness. Thus, there has been an increasing academic interest in investigating the performance of ceramic membrane supports [7].

Pore-forming agents are often used to create high apparent porosity while minimizing costs and environmental impact [8]. The pore-forming agent [9] operates on the principle that it occupies a specific amount of space in the green body, which is then removed after firing, creating pores in the space it once occupied. Numerous studies have investigated the effects of various pore-forming agents on the characteristics of ceramic membrane supports. These agents include calcium carbonate [10], carbon black [8], graphite [11], polymethyl methacrylate microspheres [12], dextrin [13], starch [14], and other materials that can decompose to produce gas at high temperatures, all of which have

specific decomposition temperature ranges. Additionally, natural or synthetic organic matter typically decomposes in the range of 200 to 300 °C.

To create pores, Mohamed et al. [15] prepared cost-effective microfiltration ceramic membranes using cassava starch and bovine bone ash as pore-forming agents at a sintering rate of 2 °C/min at 1150 °C. Dele-Afolabi et al. [16] prepared porous alumina carriers with excellent mechanical properties using corn cobs as pore forming agents at a rate of 1 °C/min. Liang et al. [13] prepared fly ash based supports for flue gas moisture recovery using dextrin as a pore forming agent at a sintering rate of 1 °C/min to 2 °C/min at 1150 °C. In a previous study, Loess-based ceramic membrane supports were prepared using CMC as a pore-forming agent. The temperature was raised at a rate of 2 °C/min from room temperature to 350 °C, followed by 4 °C/min between 350 °C and 600 °C, 1 °C/min up to 750 °C, and then at a rate of 2 °C/min after 750 °C.

As can be seen, regardless of the type of pore-forming agent utilized, it is significantly important to prevent the black center, warping, and cracking of the support during firing by restricting the pyrolysis rate during its decomposition temperature interval [17]. However, the majority of the relevant research only adds one pore-forming agent when preparing ceramic membrane supports [18], which leads to a more condensed temperature range for their firing loss and makes it challenging to regulate the pyrolysis rate. The peak gas emission can be

*Corresponding author:
Tel: +86 13186086167
Fax: 029-81369000
E-mail: guoyani2002@163.com

reduced while expanding the oxidation or decomposition temperature range if a composite pore-forming agent, or different single pore-forming agents with different decomposition temperature intervals, is used. This is conducive to reducing or even eliminating the defects of the support caused by the rapid decomposition of the pore-forming agent. In addition, the rapid firing of the support can be achieved by accelerating the heating rate.

The purpose of this study was to investigate the effects of sintering temperature [19], heating rate [20], and pore-forming agent addition [21] on the performance of fly ash ceramic membrane support prepared by the extrusion molding method. The problems caused by a single pore-forming agent, such as cracking, shorten the firing cycle of the support. The findings of this study will serve as a research foundation for the development of low-cost fly ash ceramic membrane supports made by extrusion molding.

Experimental

Raw material

Fly ash, taken from Xi'an West Suburban Power Plant, was utilized after sieving by ball milling ($d_{50}=4.25 \mu\text{m}$) [22]. Sawdust (400 mesh, Jiangmen Weihua Spice Factory), calcium carbonate (CaCO_3 , analytical purity, Tianjin Damao Chemical Reagent Factory), and hydroxyethyl cellulose (HEC, analytical purity, Shanghai Maclean Biochemical Technology Co., Ltd.) were used as composite pore-forming agents. Titanium dioxide (TiO_2 , analytical pure, Tianjin Comio Chemical Reagent Co., Ltd.) was used as the sintering aid; carboxymethyl cellulose (CMC, analytical pure, Shanghai Maclean Biochemical Technology Co., Ltd.) was used as the binder.

Preparation of the support

Fly ash:CMC:TiO₂:composite pore-forming agent = 1:0.03:0.04:0.1 (mass ratio) was mixed with the proper amount of water in a beaker and heated to 90 °C for 2 hours to create a clay that contained 15% water. This clay was then aged for 48 hours at room temperature (about 25 °C). A moist embryo with an inner diameter of 9.0 mm, an outside diameter of 15.0 mm, and a length of roughly 15.0 cm was extruded from a ceramic extrusion machine. They underwent a specific sintering regime in a muffle furnace after drying at room temperature (about 25 °C).

Characterization

The apparent porosity of the support was measured by Archimedes' drainage method. The pore size distribution and the average pore size of the support were measured by Auto Pore IV9500 mercury pressure meter. The flexural strength of the support was measured by the CMT5105 universal material testing machine by the three-point bending method with a span of 80

mm, and each sample was measured three times. The acid and alkali corrosion resistance is calculated as the mass change of the support after 24 h immersion in H_2SO_4 at pH=1 and NaOH solution at pH=13. The raw materials were analyzed thermally by a TGA/SDTA851e thermogravimetric analyzer in the temperature range of 25-1000 °C at a rate of 10 °C/min. The crystalline composition of the supports was analyzed by a D/MAX-2400 X-ray diffractometer in the scan range of 10-70° at a rate of 5 °/min. The microstructure evolution of the raw materials and the supports were analyzed by a Q45 scanning electron microscope.

Pure water flux was calculated by equation (1), measured at 25 °C, 0.1 MPa.

$$J = \frac{V}{A \cdot t} \quad (1)$$

where: J is the permeate flux, $\text{L}/(\text{m}^2 \cdot \text{h} \cdot \text{MPa})$; V is the permeate volume, L; A is the effective membrane area, m^2 ; t is the test time, h.

Experiments on optimization

Superior supports generally exhibit high permeability and mechanical properties, which can be quantified by pure water flux and flexural strength. A classical one-factor experiment was conducted to determine the optimal factorial conditions by measuring the effects of pore-forming agent content (10-18 wt%), heating rate (2-10 °C/min), and sintering temperature (950-1050 °C) on pure water flux and flexural strength. The study utilized response surface methodology (RSM) of the central composites test to determine the interaction between pore-forming agent content (A), heating rate (B), and sintering temperature (C) on pure water flux and flexural strength(BBD). The study aimed to fit the data using equations (2) and (3) as dependent variables.

$$Y = \beta_0 + \sum_{i=1}^n \beta_i X_i + \sum_{i=1}^n \beta_{ii} X_i^2 + \sum_{i=1}^n \sum_{j=i+1}^n \beta_{ij} X_i X_j \quad (2)$$

$$Y = \beta_0 + \beta_1 X_1 + \beta_2 X_2 + \beta_{12} X_1 X_2 + \beta_{11} X_1^2 + \beta_{22} X_2^2 \quad (3)$$

where Y is the predicted response (pure water flux and flexural strength), β_0 , β_i , β_{ii} , β_{ij} are the constant, linear, quadratic and interaction coefficients respectively; X_i and X_j are the dependent variables.

The study conducted 17 sets of experiments with varying values for the independent variables based on the optimal factor condition identified in the first step. Please refer to Table S1 for details.

Data analysis

The data were analyzed with Design-Expert version 13 to obtain a mathematical model for equations (2) and (3), as well as response surface and contour plots. ANOVA (analysis of variance) and diagnostic nodes were used to assess the accuracy and fit of the model.

Results and Discussion

Analysis of raw materials

The main components of fly ash are listed in Table 1. As shown in Table 1, Al_2O_3 and SiO_2 are commonly used in the preparation of ceramic membrane supports, indicating that fly ash is suitable for the preparation of supports. The surface morphologies of fly ash, sawdust and CaCO_3 and the TG curves of the three pore-forming agents are shown in Fig. 1. Fly ash is irregularly shaped, sawdust is long-fibrous, and CaCO_3 particles are small, where sawdust oxidizes or decomposes between 100 and 500 °C, calcium carbonate oxidizes or decomposes between 600 and 800 °C and HEC oxidizes or decomposes between 200 and 850 °C. These findings led to the decision to use a composite pore-forming agent with a sawdust/calcium carbonate/HEC ratio of 5/3/2.

To improve the formulation of the sintering regime

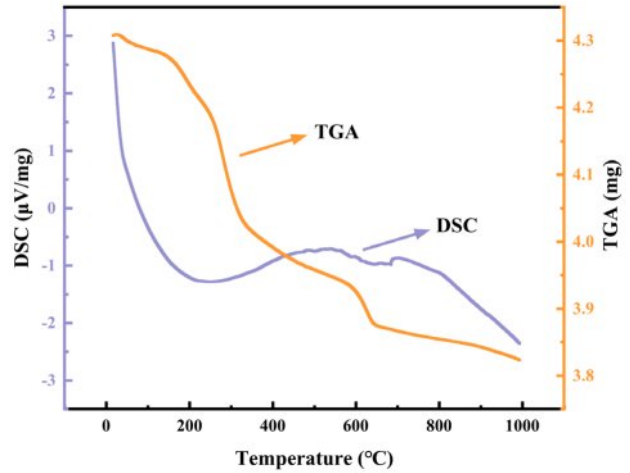


Fig. 2. TGA-DSC curves of the mixed powder with sawdust/ CaCO_3 /HEC of 5/3/2 and 11.46 wt% of the pore-forming agent.

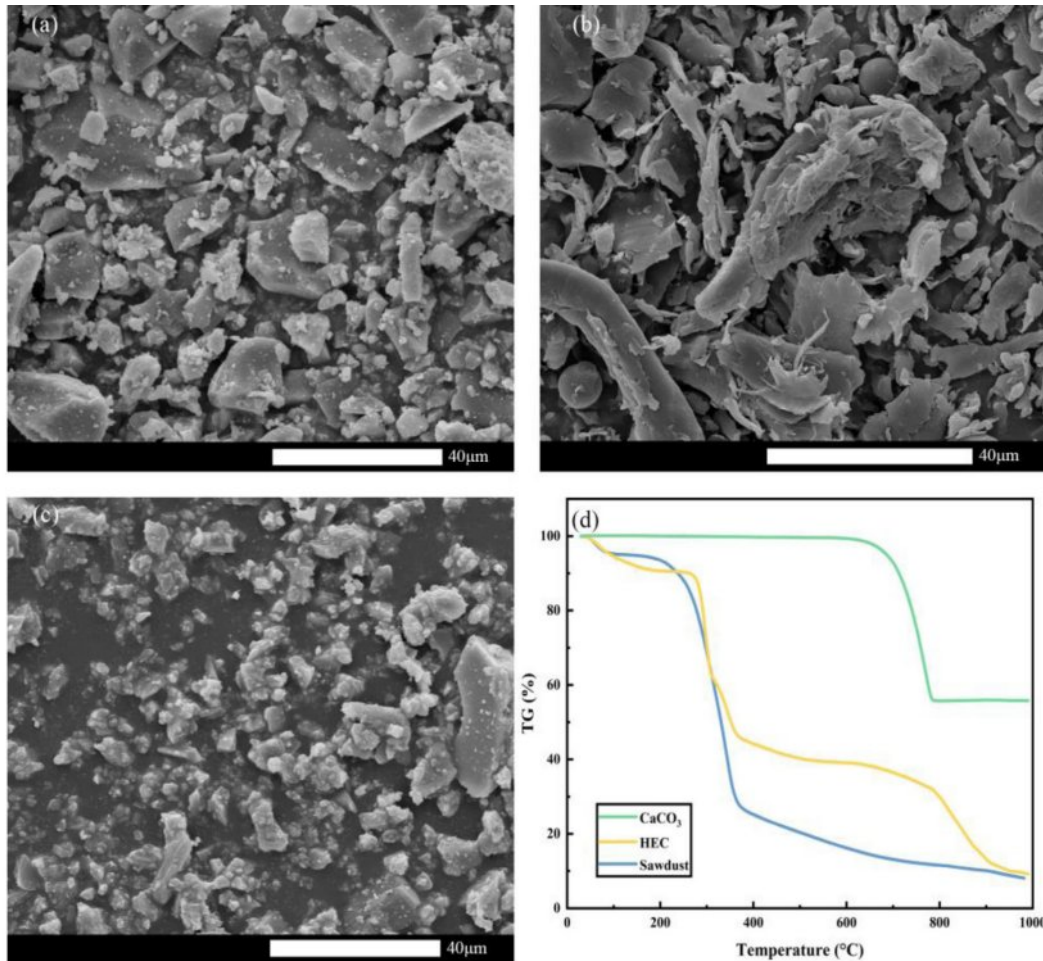


Fig. 1. Microstructure evolution of raw materials. (a) Fly ash, (b) Sawdust, (c) CaCO_3 , and (d) TG curves of the three pore-forming agents.

Table 1. Table of the chemical composition of fly ash.

Composition	SiO_2	Al_2O_3	CaO	Fe_2O_3	K_2O	Na_2O	MgO	NiO	other
wt/%	56.9	15.7	7.10	6.54	2.00	0.957	0.952	0.045	0.23

Table 2. Sintering regime of fly ash-based ceramic membrane supports.

Temperature/(°C)	25-200	200	200-700	700	700-X	X	Natural cooling
Heating rate/(°C/min)	1	/	1	/	1	/	/
Holding time/(h)	/	2	/	2	/	2	/

X: Target temperature, °C.

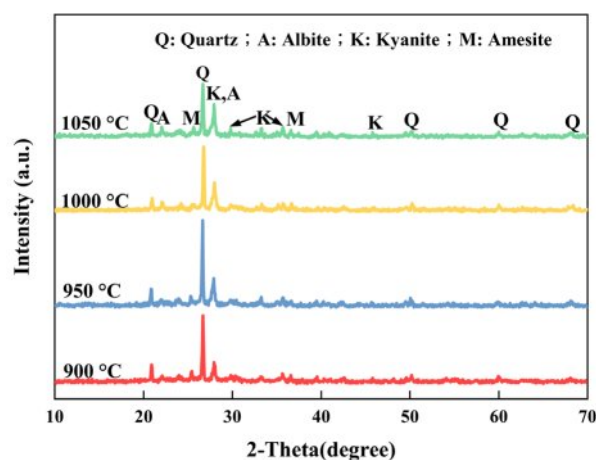
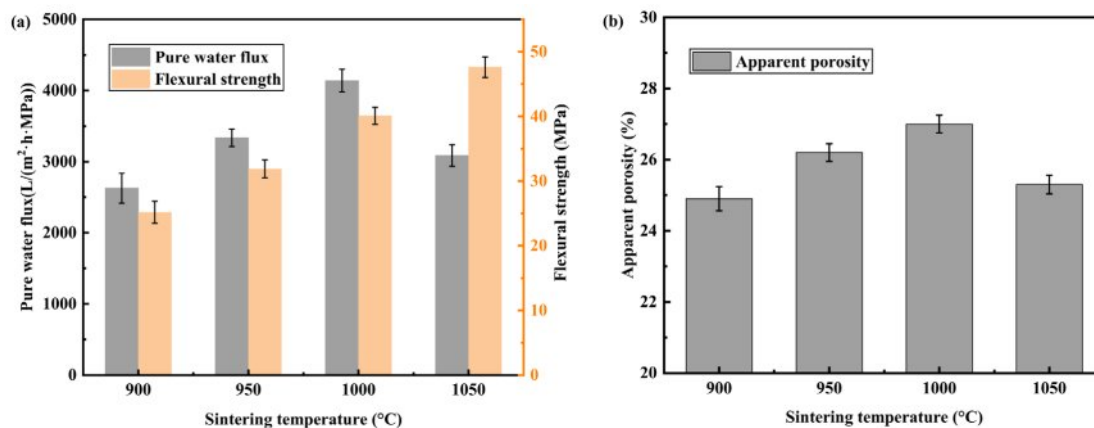
for the support, a thermal effect analysis was conducted in Fig. 2 to explore the pyrolysis temperature range of the composite porogenic agent. A portion of the dried support (11.46 wt% of composite pore maker content, with a sawdust:CaCO₃:HEC mass ratio of 5:3:2) was ground into powder and heated to 1000 °C at a rate of 10 °C/min, as depicted in Fig. 2. The composite pore-forming agent can prevent a single type of pore-forming agent from rapidly decomposing in a limited temperature range. It is possible to prevent the rapid breakdown of a single kind of pore-forming agent throughout a small temperature range. The use of fibrous sawdust makes it easier to create continuous pores that are large in size, which makes it easier to prepare ceramic membrane supports with high apparent porosity. Additionally, CaCO₃ and HEC's higher pyrolysis temperatures. The range of oxidation or decomposition temperatures is also widened by the higher pyrolysis temperatures of CaCO₃ and HEC. Thus, the supports' sintering regime was established, as shown in Table 2.

Effect of sintering temperature on the properties of the support

As seen in Fig. 3, as the sintering temperature grew, the apparent porosity of the supports and the pure water flux increased and then declined, reaching a maximum at 1000 °C, while the flexural strength continued to rise. The large improvement in flexural strength is ascribed to an enhanced degree of sintering, the generation of CaO from CaCO₃ breakdown, and a decrease in sensible porosity when the sintering temperature is raised from

1000 °C to 1050 °C, which reduces the flux of pure water. Due to the complete decomposition of the pore-forming agent, the formation of more continuous pores in the support sintered at 1000 °C, and the agglomeration of small pores into larger pores as sintering progresses, the support exhibits a higher pure water flux at 1000 °C than at 900 °C and 950 °C.

As shown in Fig. 4, Quartz, sodium feldspar, and sapphire are the three primary crystalline phases of the supports at 900–1050 °C sintering. The sodium feldspar and sapphire phases steadily grow as the sintering temperature rises, while the quartz phase increases initially before declining. This is caused by the increase

**Fig. 4.** Effect of different sintering temperatures on the XRD patterns of the support.**Fig. 3.** (a) Effect of various sintering temperatures on the pure water flux and flexural strength of the support; (b) Effect of various sintering temperatures on the apparent porosity of the support.

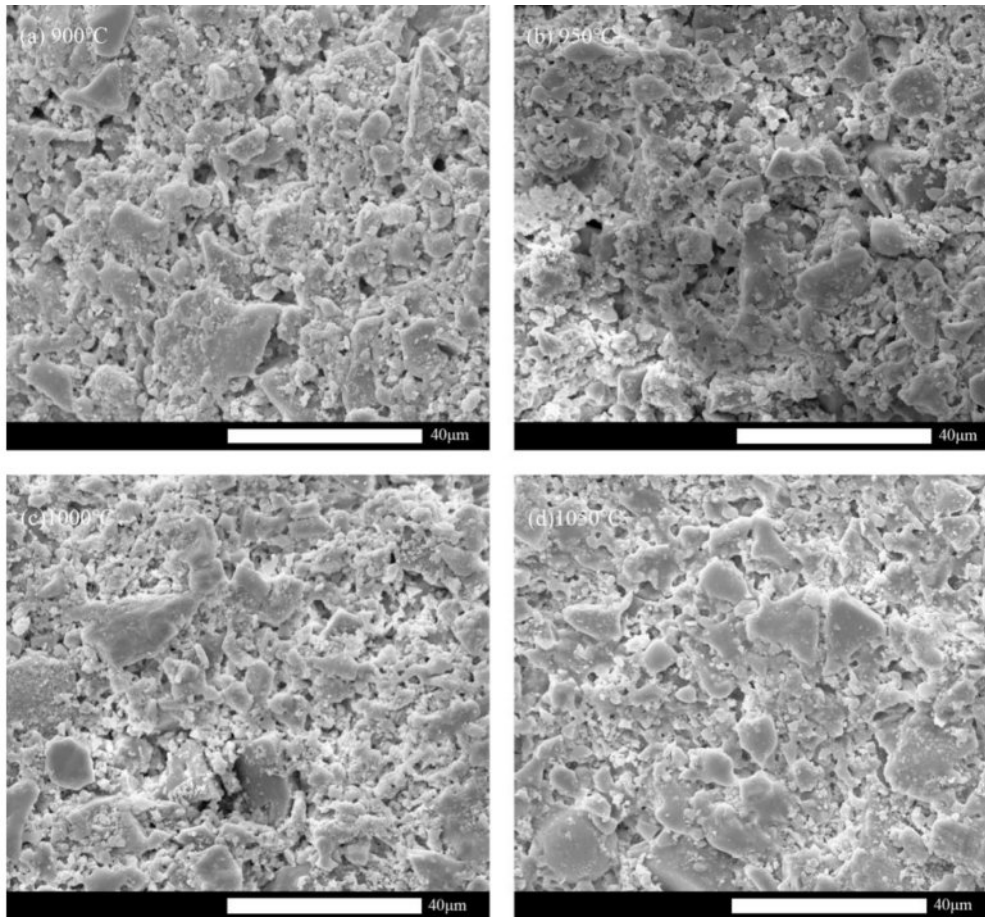


Fig. 5. Microstructure evolution at different sintering temperatures. (a) 900 °C, (b) 950 °C, (c) 1000 °C, (d) 1050 °C.

in temperature, which provides enough bonding energy for the material's deconstructive reorganization and encourages the generation of phase transitions [23]. However, an excessively high sintering temperature causes the support to severely densify, which is macroscopically manifested by poor water permeability (Fig. 3a). Low-melting point aluminosilicates and silicates, such as sodium feldspar and sapphire, are created when the alkali metal oxides (K_2O , Na_2O , etc.) present in fly ash react with SiO_2 and Al_2O_3 below 1050 °C. As a result, the degree of support densification is increased. Both soda feldspar and sapphire belong to the trigonal system, which can make the internal structure of the support show anisotropy in hardness and help improve the support's chemical stability [24].

Figure 5 depicts the support's microstructure evolution at different sintering temperatures. The edges of sintered fly ash particles become rounded and smooth in comparison to their initial morphology, showing that the melting phenomenon during the sintering process has effectively produced a neck connection between the particles. When the temperature is low, the pore structure is irregular, the flexural strength is poor, and the surface is mostly created by the direct accumulation of particles. When the temperature is too high, the support surface

exhibits the liquid phase effect, which causes the pure water flux to drastically fall. At 1000 °C, the support's liquid phase action is mild, and the porous structure offers both a decent pure water flux and a certain amount of flexural strength.

Effect of temperature increase rate and pore-forming agent content on the properties of the support

The support was prepared by adding various amounts (10 wt%, 14 wt%, 18 wt%, and 22 wt%) of the composite pore-forming agent, and the sintering system was configured as follows: starting at room temperature, the temperature was increased to 200 °C, 700 °C, and 1,000 °C at a rate of 1 °C/min, 2 °C/min, 5 °C/min, and 10 °C/min, respectively to room temperature.

As seen in Fig. 6(a)-6(c), when the heating rate is constant, the apparent porosity of the support and the pure water flux both exhibit a considerable increasing trend with the addition of more pore-forming agents, whereas the flexural strength exhibits the opposite trend. This is because sawdust and HEC are fibrous, which encourages the development of continuous pores and raises the apparent porosity of the proppant but also has a detrimental effect on flexural strength. The support's pure water flux and flexural strength tended to decline

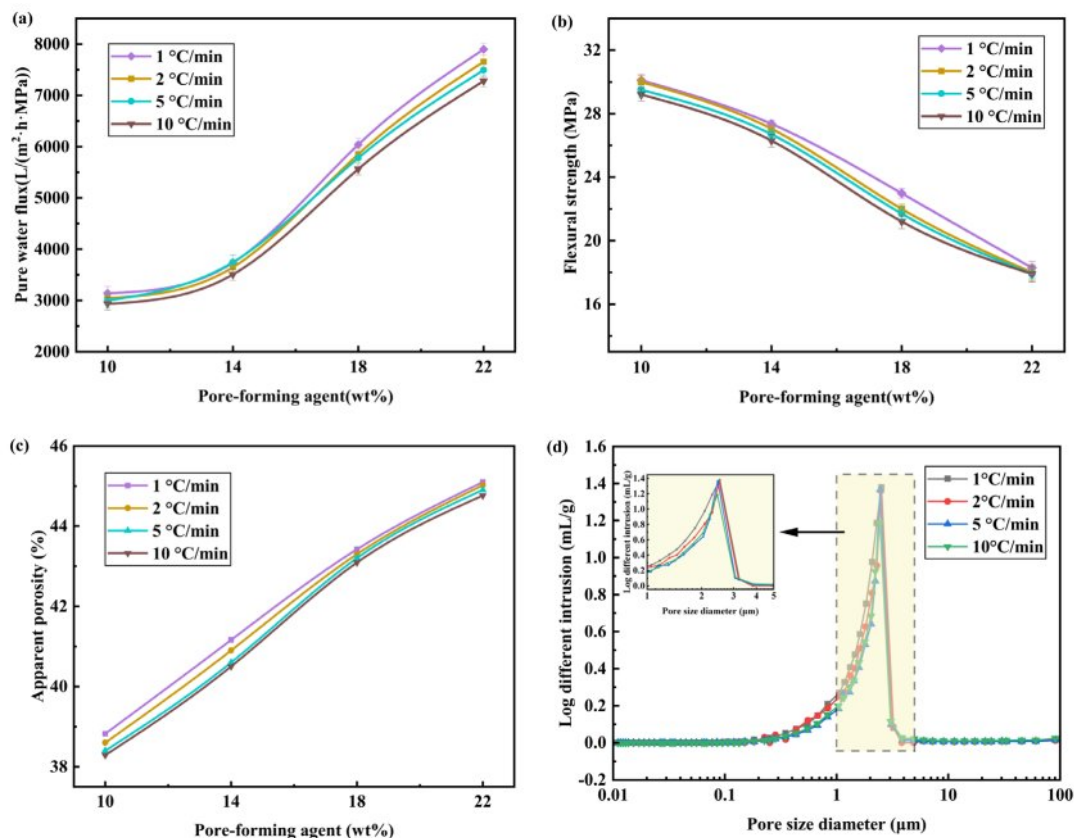


Fig. 6. Properties of supports prepared at different heating rates. (a) Pure water flux, (b) Apparent porosity, (c) Flexural strength, (d) Pore size distribution (the content of pore-forming agent was 10 wt%).

Table 3. Average pore size of supports at different heating rates (the content of pore-forming agent was 10 wt%).

Heating rate/(°C/min)	1	2	5	10
Average pore size/ (μm)	1.79	1.47	1.28	1.34

significantly with an increase in heating rate when the pore-forming content remained constant. The support's pure water flux and flexural strength were unaffected even when the heating rate was increased from 1 °C/min to 10 °C/min and the pore-forming content reached 22 wt%.

Figure 6(d) displays the support's pore size distribution for various heating rates with a 10 wt% pore-forming agent content. As can be observed, the support surfaces all have a single-peak distribution, suggesting that the distribution of pore sizes within the support is largely uniform. The peak tends to migrate to the left as the heating rate rises, indicating that the heating rate has a bigger impact on the support's pore size distribution and that the average pore size of the support somewhat lowers (as shown in Table 3).

The microstructure evolution of the supports created with various pore-forming agent additions were shown

in Fig. 7. The more pore structure is present in the support the greater the pore-forming agent content. Fig. 6(a)-6(c) shows that the apparent porosity, pure water flux, and flexural strength of the support are less affected by the heating rate. The average pore size of the support marginally reduced as the heating rate increased, as seen in Fig. 6(d) and Table 3, respectively. The performance of the support remained essentially consistent despite an increase in heating rate from 1 °C/min to 10 °C/min, which can be attributed to the composite pore-forming agent. The emission rate of gaseous by-products will increase as the heating rate rises. The flexural strength of the support will significantly decrease if the gaseous material cannot be discharged promptly because cracks will form when the gas pressure exceeds the bonding strength of the particles [25]. However, the composite pore-forming agent can effectively mitigate or even eliminate this flaw, allowing for the rapid firing of ceramic membrane supports.

Optimisation experiments

Response Surface Methodology (RSM)

The range of experimental parameters based on the independent variables (pore-forming agent content, heating rate, and sintering temperature) is shown in Table S1, and the dependent variables (pure water flux and

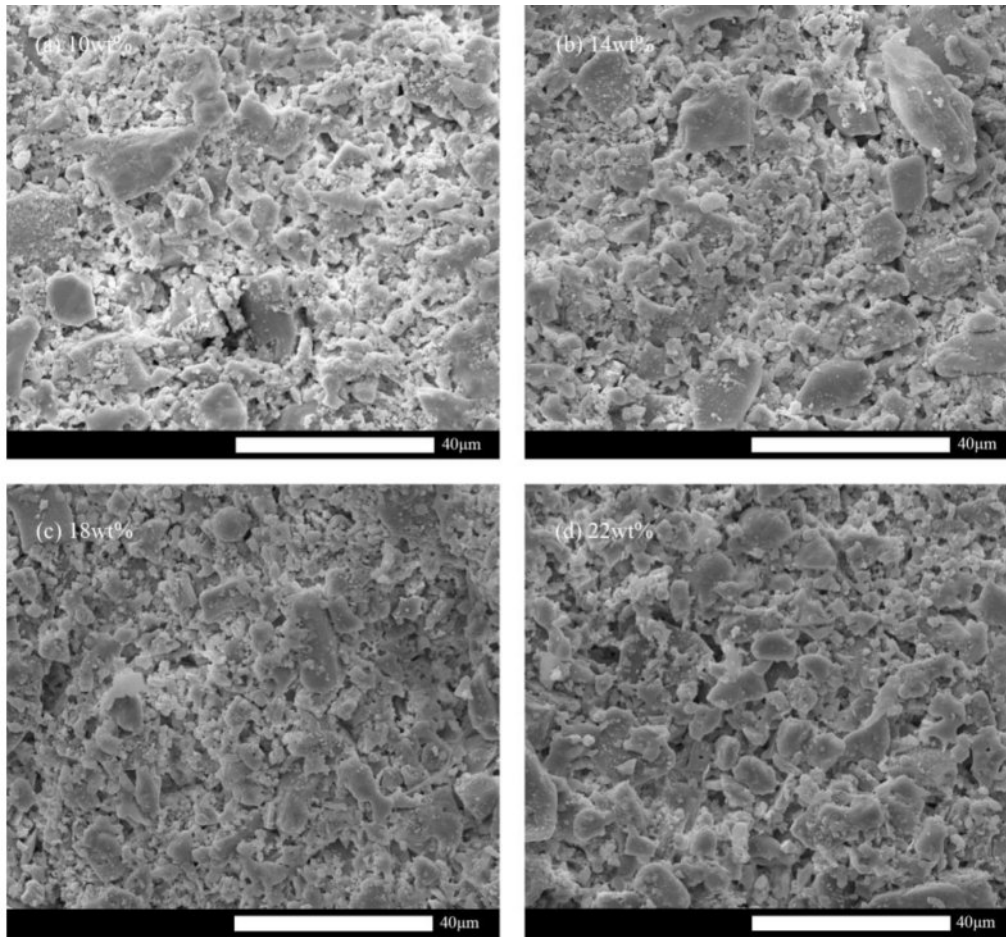


Fig. 7. Microstructure evolution under different contents of composite pore-forming agents. (a) 10 wt%, (b) 14 wt%, (c) 18 wt%, (d) 22 wt%.

Table 4. Analysis of Variance (ANOVA) predictions for the response surface of pure water flux.

Source	Sum of squares	df	Mean square	F value	p-value Prob>F		
Model	1.526E+07	9	1.696E+06	85.61	< 0.0001	significant	
A-pore-forming agent content	1.169E+07	1	1.169E+07	590.06	< 0.0001		
B-heating rate	1.913E+05	1	1.913E+05	9.66	0.0171		
C-sintering temperature	4.210E+05	1	4.210E+05	21.26	0.0025		
AB	4230.64	1	4230.64	0.2136	0.6580		
AC	31.64	1	31.64	0.0016	0.9692		
BC	7008.95	1	7008.95	0.3539	0.5706		
A ²	6.223E+05	1	6.223E+05	31.42	0.0008		
B ²	1.567E+05	1	1.567E+05	7.91	0.0261		
C ²	1.885E+06	1	1.885E+06	95.20	< 0.0001		
Residual	1.386E+05	7	19805.60			not significant	
Lack of Fit	88904.77	3	29634.92	2.38	0.2102		
Pure Error	49734.44	4	12433.61				
Standard deviation			140.73		R-Squared		0.9910
Mean			3660.56		Adjusted R-Squared		0.9794
Coefficient of Variation %			3.84		Predicted R-Squared	0.9040	
Press			1.478E+06		Adequate Prediction	34.4723	

Table 5. Analysis of Variance (ANOVA) predictions for the response surface of flexural strength.

Source	Sum of squares	df	Mean square	F value	p-value Prob>F	
Model	229.96	9	25.55	43.00	< 0.0001	significant
A-pore-forming agent content	118.77	1	118.77	199.88	< 0.0001	
B-heating rate	1.70	1	1.70	2.86	0.1344	
C-sintering temperature	99.08	1	99.08	166.74	< 0.0001	
AB	0.5097	1	0.5097	0.8578	0.3852	
AC	0.0324	1	0.0324	0.0545	0.8220	
BC	0.1451	1	0.1451	0.2442	0.6363	
A ²	0.0158	1	0.0158	0.0266	0.8751	
B ²	1.06	1	1.06	1.78	0.2242	
C ²	1.10	1	1.10	1.85	0.2157	
Residual	4.16	7	0.5942			
Lack of Fit	2.48	3	0.8267	1.97	0.2608	not significant
Pure Error	1.68	4	0.4198			
Cor Total	234.12	16				
Standard deviation			0.7709	R-Squared		0.9822
Mean			27.13	Adjusted R-Squared		0.9594
Coefficient of Variation %			2.84	Predicted R-Squared		0.8220
Press			41.66	Adequate Prediction		25.4533

flexural strength) of the optimized experimental results are shown in Table S2. The second-order polynomials obtained from the optimized experimental results are given by equations (4) and (5) of the regression model.

$$Y_1 = 3668.76 + 1226.82A - 154.63B - 232.85C - 32.03AB + 2.81AC + 41.22BC + 384.44A^2 + 209.11B^2 - 669.17C^2 \quad (4)$$

$$Y_2 = 27.01 - 3.91A - 0.4613B + 3.57C + 0.3515AB - 0.0900AC + 0.1876BC + 0.0613 + 0.5430B^2 - 0.5112C^2 \quad (5)$$

Where Y_1 = pure water flux, Y_2 = flexural strength, A = pore-forming agent content, B = heating rate, C = sintering temperature.

ANOVA results

Table 4 and 5 confirm the validity of equations (4) and (5) through analysis of variance (ANOVA). The p-values of the models were calculated to be less than 0.0001, indicating a good fit. The lack of fit's p-values of 0.2102 and 0.2608 are not significant, indicating that the error is not significantly larger than the pure error and the model is acceptable. The model is a good fit, as indicated by the predicted R-Squared of 0.9040 and 0.8220, and the adjusted R-Squared of 0.9794 and 0.9594, even after considering the model's complexity and the number of independent variables. The difference in the adjusted R-Squared is not significant.

Figures 8(a) and 9(a) indicate that the points in the

plots of normal residuals are close to the diagonal line. This suggests that the explicit residuals are approximately normally distributed and that the assumption of normal distribution of the model is valid. Phylogenetic plots of residuals versus predicted values are presented in Fig. 8(b) and Fig. 9(b). The plots show that all points fall within a narrow horizontal band and that the residuals have a consistent distribution. These results indicate that equations (4) and (5) are consistent with the experimental data and satisfy the model's assumptions. Figs. 8(c) and 9(c) show the residuals versus multiple runs, indicating that the samples are independent and do not interact with each other. Figs. 8(d) and 9(d) display diagnostic plots of predicted and actual values of pure water flux and stent flexural strength. The scatter plot points are densely distributed on a straight line, indicating the high accuracy of the predictive model. Therefore, this regression model is suitable for optimizing the dependent variable across a range of independent variable parameters.

Three-dimensional (3D) response surface analysis

Figure 10 shows the results of a regression analysis performed using Design Expert software to determine the response surface of each variable and its interaction on pure water flux and flexural strength. Figs. 10(a) and 10(b) highlight the range of values of the factors corresponding to high pure water flux and flexural strength. The analysis indicates that factor A has a significant effect on the properties of the support, which is also confirmed by Tables 4 and 5. Conversely, factor B has little effect on the properties of the support and

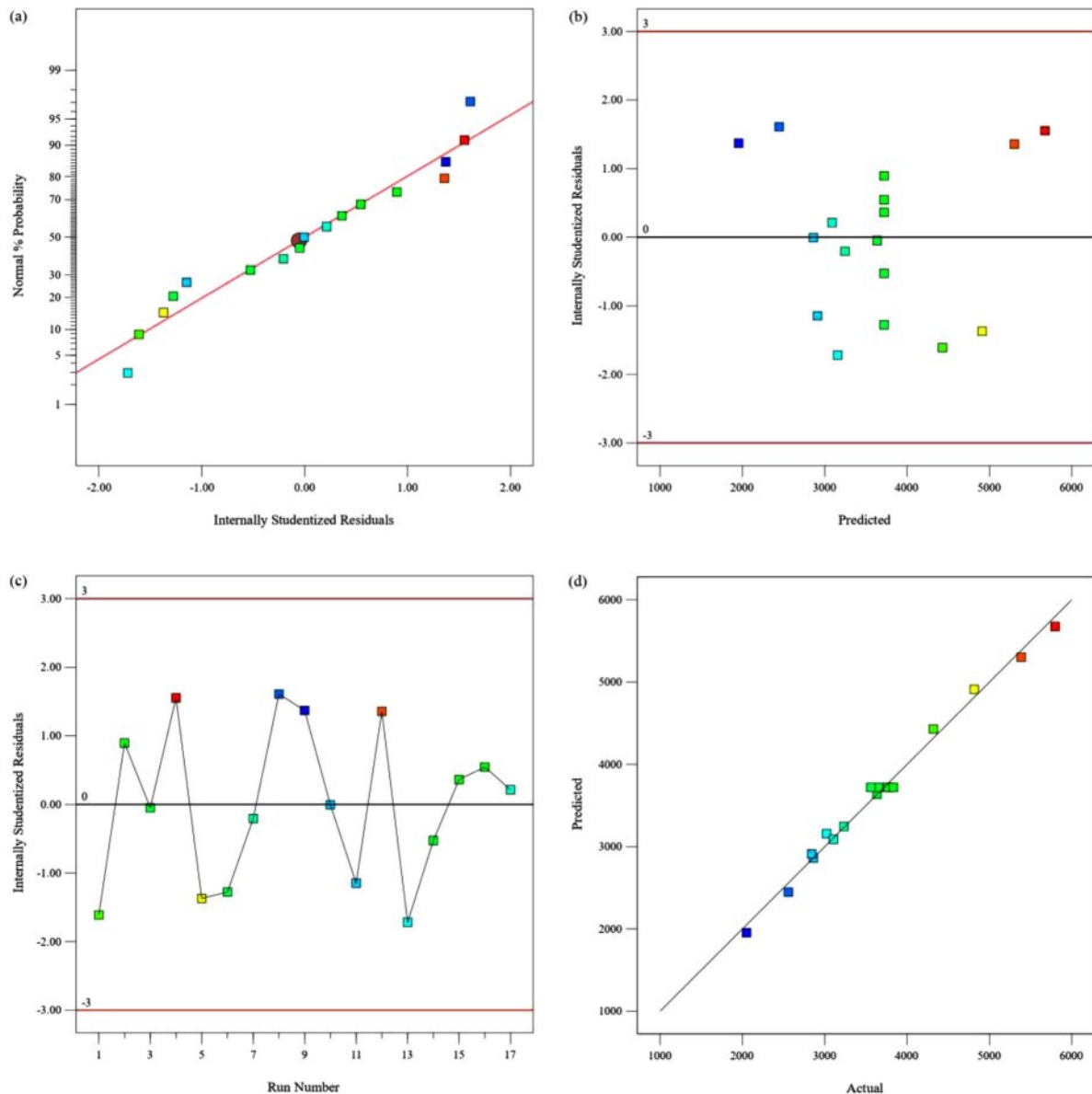


Fig. 8. Diagnostics Plots of Pure water flux, (a) Normal Plot of Residuals, (b) Residuals Versus Predicted, (c) Residuals Versus Run Number, (d) Predicted Versus Actual.

is not significant, which is consistent with the findings above. The data in figure (c) indicates that increasing the amount of porogenic agent has a positive impact on the pure water flux of the support. Additionally, excessively high sintering temperatures can cause the support to slough, which negatively affects its properties. Fig. 10(d) illustrates that the positive impact of porogenic agent content on flexural strength decreases. Additionally, an increase in sintering temperature results in higher flexural strength due to the production of the liquid phase. Figs. 10(e) and 10(f) demonstrate that the interactions between factors A and C are insignificant, further confirming that the rate of temperature increase does not significantly affect the support body's performance. Table 6 shows the predicted pure water flux and flexural strength of the supports prepared under optimal conditions of

poro-forming agent content, heating rate, and sintering temperature. The errors between predicted and actual values for pure water flux and flexural strength are 1.95% and 1.31%, respectively.

Optimal sample characterisation

The average pore size of the support is 1.88 μm , as shown in Fig. 11. The support was produced under optimal conditions, with a pore-forming agent content of 11.46 wt%, a heating rate of 10 $^{\circ}\text{C}/\text{min}$, and a sintering temperature of 1020.69 $^{\circ}\text{C}$. To assess its chemical stability, the microstructure evolution of the support before and after corrosion was observed using scanning electron microscopy, and its crystal phase composition was detected.

One of the main drivers of the industrialisation of

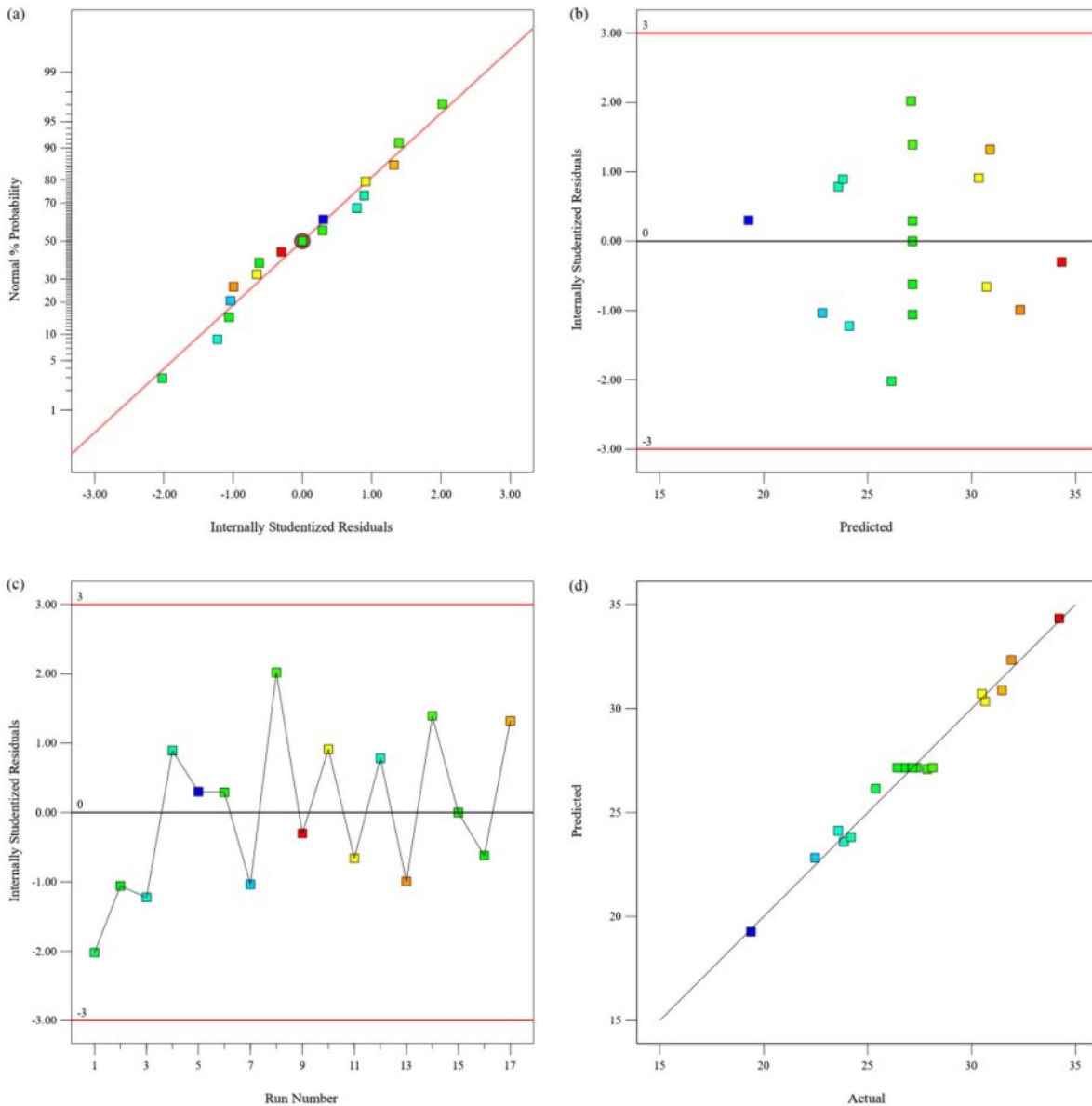


Fig. 9. Diagnostics Plots of Flexural strength, (a) Normal Plot of Residuals, (b) Residuals Versus Predicted, (c) Residuals Versus Run Number, (d) Predicted Versus Actual.

ceramic membrane supports is their chemical stability. The supports' mass loss was retained at a respectably low level while being sintered at 1000 °C, as shown in Fig. 12(a), and the acid-base loss rate after 24 hours was 2.064%/0.233%, respectively. The acid-base mass loss rates were less than 3% indicating that the prepared supports have good chemical stability. The significant number of alkali metal oxides in the fly ash that readily react with the acid may be the cause of the slightly larger mass loss of the supports in the H₂SO₄ solution compared to the NaOH solution [26]. The crystalline phase composition of the supports remains almost unchanged, as shown in Fig. 12b. Figs. 13a-13c show that the surface of the support does not change much after acid and alkali corrosion, indicating that the prepared fly

ash-based ceramic membrane support has excellent acid and alkali corrosion resistance. The tubular fly ash based inorganic ceramic membrane support is made as shown in Fig. 13(d).

Conclusions

(1) One possible technique for creating high-performance supports and accelerating their firing is the use of composite pore-forming agents. The composite pore-forming agent reduces the overall sintering energy consumption of the ceramic membrane, thus lowering the cost of preparation, by shortening the firing cycle without affecting the support's performance.

(2) The study investigated the impact of sintering

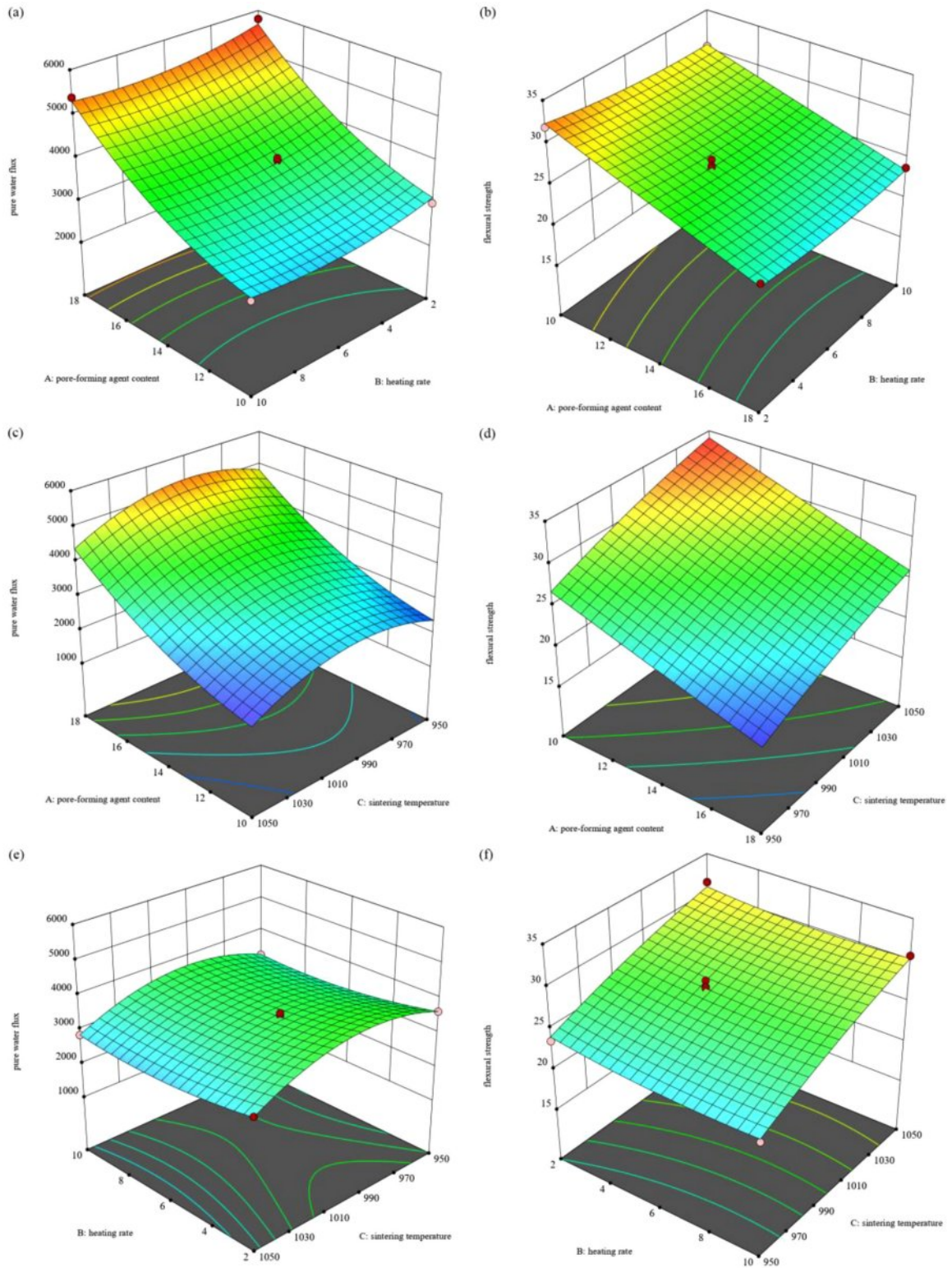


Fig. 10. Response surface analysis of different factors.

Table 6. Predicted and actual values of pure water flux and flexural strength under optimal conditions.

Pore-forming agent content (wt%)	Heating rate (°C/min)	Sintering temperature (°C)	Pure water flux (L/(m ² ·h·MPa))		Flexural strength (MPa)	
			Predicted	Observed	Predicted	Observed
11.46	10.00	1020.69	2925.54	2983.81	30.86	31.27

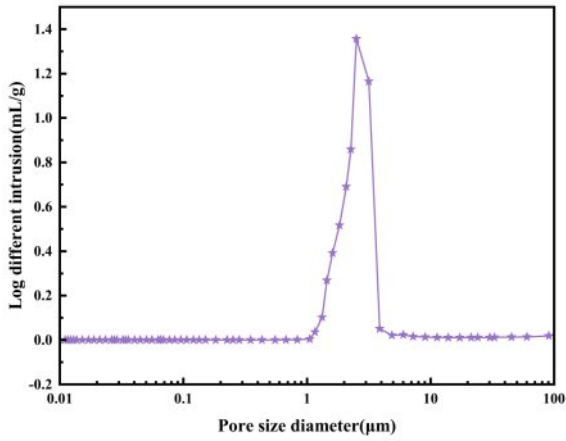


Fig. 11. Pore size distribution.

temperature, pore-forming agent content, and heating rate on the performance of an inorganic ceramic membrane support made from fly ash. Response values, including pure water flux and flexural strength, were optimized using BBD's RSM. The fly ash-based support exhibited high permeability, mechanical strength, and chemical stability when sintered at 1020.69 °C, with a pore-forming agent content of 11.46 wt% and a heating rate of 10 °C/min. The ceramic membrane support developed

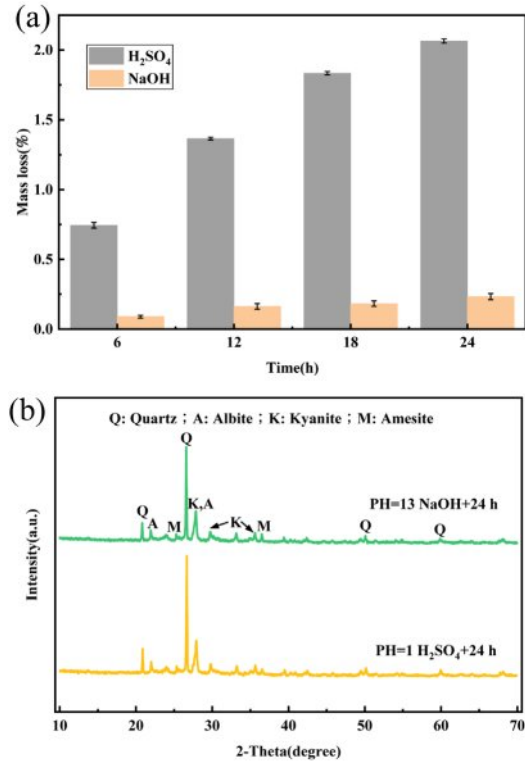


Fig. 12. Acid and alkali corrosion resistance. (a) Mass loss after acid and alkali corrosion, (b) XRD after acid and alkali corrosion.

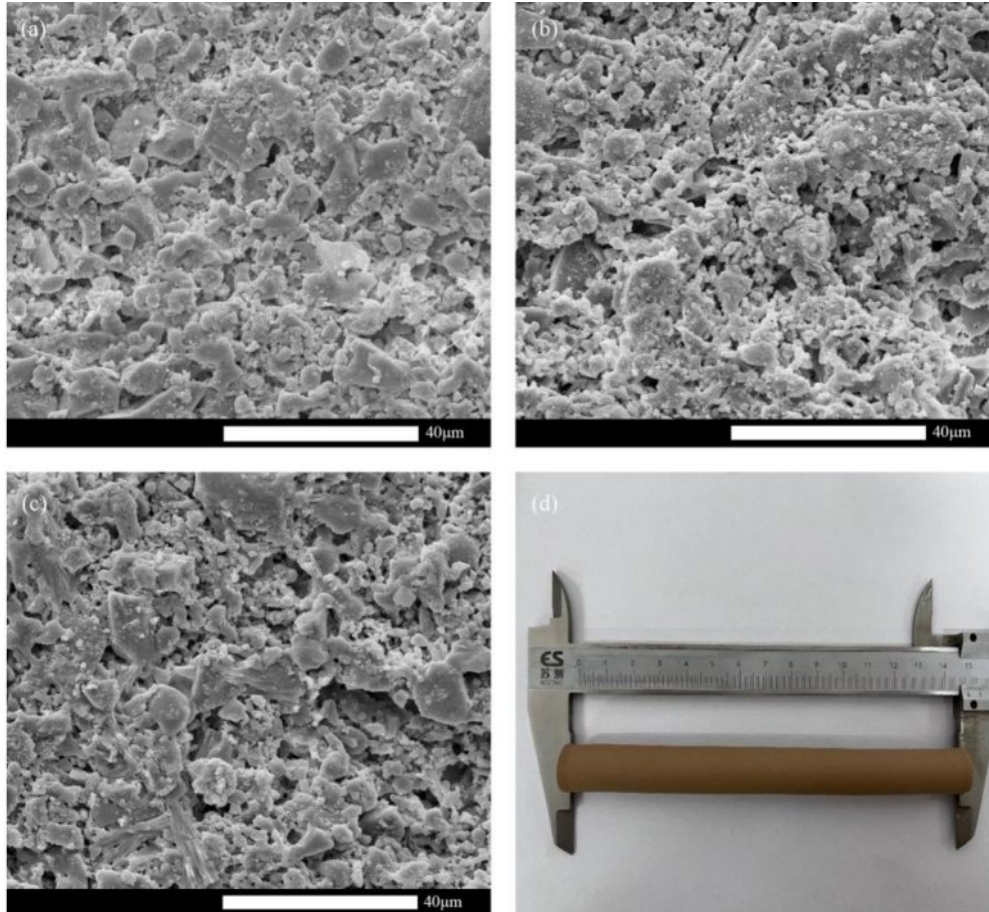


Fig. 13. SEM images of the support (a) before corrosion, (b) after acid corrosion, (c) after alkali corrosion, and (d) Physical picture.

in this study has practical applications due to its high pure water flux of 2983.81 L/(m²·h·MPa), impressive flexural strength of 31.27 MPa, low acid-alkali loss rate of 2.064%/0.233%, and average pore size of 1.88 μm.

Acknowledgments

This work received financial support from the Key R&D Project of Shaanxi Provincial Department of Science and Technology (No. 2020ZDLNY06-09) and the Special Research Project of Shaanxi Provincial Department of Education (No. 22JK0393).

Conflicts of Interest

The authors declare no conflict of interest.

Data availability statement

All data that support the findings of this study are included within the article (and any supplementary files).

References

1. Y. Li, W. Cao, L. Zhao, and D. Liu, *J. Appl. Ceram. Technol.* 19[4] (2022) 2093-2103.
2. B.A. Mahassen, M. Khaled, H. Noureddine, and S. Ezzedine, *J. Appl. Ceram. Technol.* 19[4] (2022) 2114-2123.
3. K. Cho, Y. Jeong, K.W. Seo, and S. Lee, *Bioresour. Technol.* 256 (2018) 137-144.
4. P. Bhattacharya, D. Mukherjee, N. Deb, and S. Swarnakar, *J. Environ. Chem. Eng.* 8[3] (2020) 103803.
5. Z.Q. Li, Y.L. Ren, J.Z. Hao, and J. Xu, *J. Ceram. Process. Res.* 25[3] (2024) 389-403.
6. Z. Tong, G.R. Zhou, J.Y. Wang, and T. Liu, *J. Environ. Eng.* 13[7] (2019) 1550-1556 (in Chinese).
7. Z. Tong, J.X. Zhang, X.J. Sun, and B.W. Yang, *Mater. Rev.* 34[12] (2020) 12050-12056 (in Chinese).
8. Y.F. Cheng, Y.G. Yu, C. Peng, and J.Q. Wu, *Ceram. Int.* 46[8] (2020) 11297-11303.
9. D.H. Liang, J.G. Huang, H. Zhang, and H.M. Zhang, *Ceram. Int.* 47[8] (2021) 10464.
10. F. Jiang, L.L. Zhang, E. Mukiza, and Z.W. Qi, *J. Alloy. Compd.* 749 (2018) 750-757.
11. K. P. Huang, Z. Tong, B.W. Yang, and X.J. Sun, *J. Funct. Mater.* 51[3] (2020) 3144-3149 (in Chinese).
12. M. M. Bazin, N. Ahmad, and Y. Nakamura, *J. Asian. Ceram. Soc.* 7[4] (2019) 417-425.
13. D.H. Liang, J.G. Huang, Y.T. Zhang, and Z. Zhang, *J. Eur. Ceram. Soc.* 41[11] (2021) 5696-5710.
14. J.J. Liu, Y.B. Li, Y.W. Li, and S.B. Sang, *Ceram. Int.* 42[7] (2016) 8221-8228.
15. M. Mouafon, D. Njoya, M. Hajjaji, and A. Njoya, *Trans. Indian Ceram. Soc.* 79[1] (2020) 1-12.
16. T.T. Dele-Afolabi, M.A. Azmah Hanim, O.J. Ojo-Kupoluyi, and R. Calin, *J. Appl. Ceram. Technol.* 18[1] (2021) 244-252.
17. M. Zhou, W.B. Dai, and L.K. Zeng, *J. Ceram. Process. Res.* 16[5] (2015) 490-494.
18. Y.H. Choi, S. Kang, J. Wackerl, and K.T. Lim, *J. Ceram. Process. Res.* 14[2] (2013) 153-158.
19. A.E. Pramono, M. Z.i Nura, J.W.M. Soedarsono, and N. Indayaningsih, *J. Ceram. Process. Res.* 20[4] (2019) 333-346.
20. H.L. Lian and R.X. Cheng, *J. Ceram. Process. Res.* 20[5] (2019) 479-483.
21. J.G. Huang, H.P. Chen, R. Qi, and J.H. Yang, *J. Environ. Chem. Eng.* 11[3] (2023) 109929.
22. H. Wang, Z. Tong, Xi'an. Polytechnic. University. Master. Thesis. 2023.
23. Y.F. Cheng, Y.G. Yu, C. Peng, and J.Q. Wu, *Ceram. Int.* 46[8] (2020) 11297-11303.
24. M. Okrusch and H.E. Frimmel, *Crystals, Mineralogy*, Springer, Berlin, Heidelberg (2020) p. 3.
25. S. Wang, G. Lloyd, M. Julius, and D. Brianna, *Constr. Build. Mater.* 316 (2022) 125828.
26. B.Q. Li, X. Xie, J.F. Lv, and H. Zhu, *Conservation and Utilization of Mineral Resources* 40[5] (2020) 153-160 (in Chinese).